Food Chemistry: X 19 (2023) 100777

Contents lists available at ScienceDirect

Food Chemistry: X

journal homepage: www.sciencedirect.com/journal/food-chemistry-x

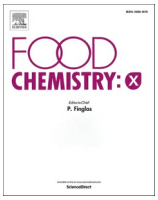

Dried grape pomace with lactic acid bacteria as a potential source for probiotic and antidiabetic value-added powders

Larisa Anghel [a], Adelina Ștefania Milea [a], Oana Emilia Constantin [a], Vasilica Barbu [a], Carmen Chițescu [b], Elena Enachi [a,b], Gabriela Râpeanu [a], Gabriel – Dănuț Mocanu [a,*], Nicoleta Stănciuc [a,*]

[a] Faculty of Food Science and Engineering, Dunărea de Jos University of Galați, 800008 Galați, Romania
[b] Faculty of Medicine and Pharmacy, Dunărea de Jos University of Galați, 800008 Galați, Romania

ARTICLE INFO

Keywords:
Red grape pomace
Drying kinetics
Convective
Infrared
Lactic acid bacteria
Antidiabetic potential

ABSTRACT

Two drying methods (convective (CD) and infrared (IR)) on grape pomace with probiotics were analysed, based on kinetic models and survival rate. The moisture ratio decreases linearly with drying time. The IR drying time reduced up to 14.3% at 50 °C. The Page model allowed to calculate the drying constant (0.188–0.404 s^{-1}), whereas the effective moisture diffusivity ranged from 6.64 × 10^{-9} to 9.38 × 10^{-9} m^2/s for CD and from 8.83 × 10^{-9} to 11.16 × 10^{-9} m^2/s for IR, respectively. Chromatographic analysis highlighted the presence of 28 anthocyanins, with cyanidin-3-*O*-monoglucoside as a main bioactive in both powder. The probiotic survivale rate reached 7.0 log CFU/g dry weight after 14 days of storage at 4 °C. The extracts affected conformation of α-amylase, with binding constants lower for IR extract (15.94 ± 1.61 × 10^{-2} Mol/L) when compared with CD (25.09 ± 2.14 × 10^{-2} Mol/L). The IC_{50} values were significant higher for the IR (6.92 ± 0.09 μMol C3G/mL) when compared with CD extract (10.70 ± 0.12 μMol C3G/mL).

1. Introduction

The traditional winemaking process from fermented grapes generates large amounts of by-products, consisting of as pomace, skin, stem and seed (Muhlack, Potumarthi, & Jeffery, 2018). Grape pomace (GP) is the principal solid residue of wine industries, generated after the grapes pressing and fermentation process. It has been estimated that around 20% of whole grapes are generated as pomace (Kammerer et al., 2004). Worldwide, wine industry generates more than 10 Mt of grape pomace (GP) annually. GP is one of the richest in bioactive compounds, including organic acids (malic acid, tartaric acid) (Sui et al., 2014), dietary fiber (up to 85%, depending on grape variety) (Nakov et al., 2020), polyphenols (near 70%) (Monteiro et al., 2021), being widely studied as an important source of bioactive for medicine and pharmacology applications, for crop protection (Teplova et al., 2018), food-grade antioxidants, as natural candidates for replacing synthetic substances, as nutraceuticals, etc. Although, GP is a rich source of antioxidants, the main drawback is their low stability. GP is very perishable due to its high-water content (75–80%) and the possible presence of residual sugars, making this by-product accessible to microbial population growth and thermal decomposition (Demirkol and Tarakci, 2018). Additionally, another critical issue is the large production of GP in a short period of time, which requires immediate stabilization to facilitate further processing and bioactive recovery (Guaita et al., 2021). Drying is the oldest preservation method, considered as an important and necessary process to prevent chemical and physical changes during storage (Guaita et al., 2021). Drying can be considered the most important step to use GP as a constituent to obtain novel food products (Demirkol and Tarakci, 2018). From the perspective of further processing of the GP, drying brings numerous advantages, such as extending the storage life, facilitating handling and reducing transport costs. In addition, drying facilitates further processing such as grinding to improve extraction yields of bioactive compounds (Mujumdar, 2006). Although it has negative effects on product quality, the hot air convective drying technique is usually used for fruit pomace drying (Taşeri et al., 2018). As alternatives, the convective hot air drying (CD) and infrared (IR) heating have gained popularity due to selected benefits such as: uniform drying, high drying rate, reduced time for processing, low energy consumption

* Corresponding authors at: Dunarea de Jos University of Galati, Faculty of Food Science and Engineering, Domnească Street 111, Building E, Room E208, 800201 Galati, Romania.
E-mail addresses: Danut.Mocanu@ugal.ro (G.D. Mocanu), Nicoleta.Stanciuc@ugal.ro (N. Stănciuc).

https://doi.org/10.1016/j.fochx.2023.100777
Received 24 April 2023; Received in revised form 26 June 2023; Accepted 28 June 2023
Available online 30 June 2023

and improved quality of the of products (Vishwanathan et al., 2013). *Lactobacillus casei* ssp. *paracasei* is a mesophilic facultative and obligate hetero-fermentative lactobacilli species, with probiotic properties, such in reducing the effects of antibiotic, norovirus and radiation-induced diarrhea, management of acute gastroenteritis (Scartoni et al., 2015), etc. Some other clinical trail revealed the effectives of probiotic treatment in reducing the small bowel injuries induced by chronic low-dose aspirin (Endo et al., 2011), orocecal intestinal transit time (Malpeli et al., 2012), etc. Therefore, the aim of this study was to study the CD and IR drying kinetics of red GP inoculated with a commercial culture of *Lactobacillus casei* ssp. *paracasei* (*L. casei* 431®) in order to enhance the functional properties of the GP. The effects of drying methods and temperatures on drying kinetics, bioactive contents, antioxidant activity and color changes of Băbească Neagră GP enriched with lactic acid bacteria were studied. The results were correlated with the probiotic viable cells. Based on the above-mentioned results, two powders were selected to extend the phytochemical profile on chromatographic method basis and the potential inhibitory effect on metabolic syndrome associated enzyme (α-amylase) on fluorescence and spectrophotometric basis. The powders obtained by drying at 45 °C were subjected to repeated extraction in order to enhance the phytochemical content and used in ultra-high-performance liquid chromatography (UHPLC), spectral analysis and in α-amylase binding studies.

2. Materials and methods

2.1. Reagents

2,2-Diphenyl-1-picrylhydrazyl (DPPH), 6-hydroxy-2,5,7,8-tetramethylchromane-2-carboxylic acid (Trolox), α-Amylase from *Aspergillus oryzae* (~1.5 U/mg), potassium persulfate ($K_2O_2S_8$), ethanol, glacial acetic acid (CH_3COOH), Folin–Ciocalteu reagent, gallic acid, sodium carbonate (Na_2CO_3), sodium nitrite ($NaNO_2$), aluminum chloride ($AlCl_3$), sodium hydroxide (NaOH) 1 M, hydrochloric acid (HCl), potassium chloride (KCl), sodium acetate (CH_3COONa), chloroform, and methanol (HPLC grade), Plate Count Agar, MRS agar, MRS broth, were purchased from Sigma-Aldrich (MilliporeSigma, Steinheim, Germany). The reference biologically active compounds standards used for the identification and quantification were also purchased from Sigma-Aldrich (MilliporeSigma, Steinheim, Germany). The commercial culture *Lactobacillus casei* ssp. *paracasei* (*L. casei* 431®) was provided by Chr. Hansen (Hoersholm, Denmark).

2.2. Plant material

Red GP of grapes variety Băbească neagră, harvested in 2021, was obtained from the Research and Development Institute for Viticulture & Oenology Bujoru, Dealul Bujorului vineyard, Galati County, Romania, in November just after cold press juicing. Before experiments, the GP was stored in a freezer at −20℃ in plastic bags. One day before each drying experiment, the required quantity of GP was taken out from the freezer and thawed in the cooler at temperature 4-6℃. The initial moisture content of grape pomace was 75.06 ± 0.43%.

2.3. Strain and growth conditions

L. casei 431® inoculum of 9.1 log CFU/mL was dispersed across the vegetal matrix. Lactic acid bacteria cell counts were assessed using a culture technique on double-layer MRS agar in duplicates for 14 days using suitable dilution. The plates were incubated for 72 h at 37 °C, with the results expressed as log CFU/g.

2.4. Purée preparation

An amount of GP with seeds (700 g) was mixed with 200 mL of double distilled water for 30 min using a food processor Philips HR2100/40. Given the initial CFU/mL of the *L. casei* 431® inoculum of 9.1 log, the probiotic was added into GP purée samples at a concentration of 1%, in order to allow a good cells survival during drying. Three variants of GP purée were obtained, coded as follows: BN_0 - fresh GP purée sample, BN_{CD} - GP purée dried by CD, BN_{IR} - GP purée dried by IR drying.

2.5. Experimental procedure

The CD and IR drying of GP purée samples were carried out in an infrared-convective dryer with 5 perforated trays (mesh trays) (Concept SO4000 Infra 500 W, Chocen, Czech Republic). The drying process was carried out at 40 °C, 45 °C and 50 °C air temperature, at a constant air velocity of 1 m/s and relative humidity of 11.2%. Air velocity was determined by a VT 115 hotwire thermo-anemometer (Kimo Instruments, Millgrove, Ontario, Canada), while the relative humidity was determined with a thermo hygrometer EE33 Series, fitted with a sensing probe (E + E Electronik Ges.m.b.H. Engerwitzdorf, Austria). Approximately 150 g of sample was spread on the tray surface to obtain a 1.5 mm thick layer. The layer thickness was measured using a digital micrometer Mitutoyo IP65 (Mitutoyo Austria GmbH). During drying, the moisture loss was recorded at 30 min intervals. A digital balance Precisa EP 125SM (Precisa, Iasi, Romania), with 0.01 g accuracy was used to record the sample weight. The drying process was finished when the GP purée sample weight reached a constant value. After drying, the products were cooled under laboratory conditions and stored in airtight containers at room temperature.

2.6. Mathematical modelling of drying curves

The moisture ratio (MR) and drying rate (DR) of GP puree samples during drying experiments were calculated using Eq. (1) and Eq. (2) (Ross et al., 2020):

$$MR = \frac{M_t - M_e}{M_0 - M_e} = \frac{8}{\pi^2} exp\left(-\frac{\pi^2 D_{eff} t}{L^2}\right) \quad (1)$$

$$DR = \frac{M_{t+dt} - M_t}{dt} \quad (2)$$

where M_t is the moisture content at t time; M_0 is the initial moisture content; M_e is the equilibrium moisture content; t is the drying time (s); D_{eff} is the effective diffusivity (m^2/s); L is the half-slab thickness (half bed thickness, (m)); M_{t+dt} is the moisture content at $t + dt$ time (g water/g dry matter); and dt is the time elapsed for drying. Experimental MR values vs drying time (t) can be represented using three semitheoretical thin layer drying models, which are widely used to model the drying kinetics of most food products and biological materials. The selected mathematical models are illustrated in Table 1 (Supplementary material). Nonlinear regression analysis were used to obtain the model parameters, R^2 (coefficient of determination) and SSR (sum of the squared residual), using the CurveExpert Professional software version 2.7.3 (free trial).

2.7. Moisture effective diffusivity and activation energy

Using the method of slopes, the moisture effective diffusivity can be calculated through Eq. (1). The effective diffusivities are typically determined by plotting experimental drying data in terms of *ln(MR)* versus time, yielding Eq. (3), and a straight line with a slope k and Eq. (4) was obtained (Ross et al., 2020):

$$\ln(MR) = ln\left(\frac{8}{\pi^2}\right) - \left(\frac{\pi^2 D_{eff} t}{L^2}\right) \quad (3)$$

$$k = \frac{\pi^2 D_{eff} t}{L^2} \quad (4)$$

Activation energy (E_a) was estimated by using Arrhenius equation (Eq. (5) from the moisture effective diffusivity (D_{eff}):

$$D_{eff} = D_0 exp\left(-\frac{E_a}{RT}\right) \quad (5)$$

where D_0 is the pre-exponential factor of the Arrhenius equation in m^2/s; E_a is the activation energy in kJ/mol; R is the universal gas constant in kJ/mol·K, (R = 8.314 J/mol·K); T is drying temperature in °K. The E_a can be determined from the method of slopes of the Arrhenius plot (Eq. (6):

$$ln\left(D_{eff}\right) = ln(D_0) - \frac{E_a}{RT} \quad (6)$$

The slope of the line is ($-E_a/R$) and the intercept equals $\ln(D_0)$ (Ross et al., 2020).

2.8. Phytochemical extraction

An amount of 0.5 g of the dried GP samples was extracted with 4.5 mL of 70% ethanol and 0.5 mL of glacial acetic acid. The extraction was performed using a sonication water bath at 30 °C for 30 min, followed by centrifugation at 6000 rpm for 10 min at 4 °C. The supernatant was characterized in terms of total monomeric anthocyanins content (TAC), total polyphenols content (TPC), total flavonoids content (TFC), and antioxidant activity. Further, for the selected powders, the extraction was repeated three times with the aim of depleting the GP in bioactive compounds.

2.9. Total monomeric anthocyanins, flavonoids and polyphenolic contents

Spectrophotometric methods were used to evaluate the phytochemicals. Therefore, the pH-differential method was used to evaluate the TAC and expressed as mg of cyanidin-3-*O*-glucoside equivalents (C3G) per g dry weight (DW). To measure the TFC, the $AlCl_3$ based method was applied and the results were expressed as mg of catechin equivalents (CE) per g dry weight (DW). The Folin-Ciocalteau's method was performed for TPC, by using a gallic acid stardard curve, allowing to express the results as mg gallic acid equivalents (GAE) per g DW.

2.10. Antioxidant activity

The ability of the fresh and dried GP samples to scavenge the DPPH radical was used to express the antioxidant activity. Volumes of 0.1 mL of extracts were mixed with 3.9 mL methanolic DPPH solution (0.1 M) and allowed to react at room temperature for 30 min, in the dark. The absorbances were read at the wavelength of 515 nm, using an UV–visible spectrophotometer (Biochrom Libra S22 UV/Vis, Cambridge, UK). The results were expressed as mMol of Trolox equivalent (TE) per g DW.

2.11. Colorimetric analysis

The colours of the fresh and dried GP samples were analysed using a MINOLTA Chroma Meter CR-410 (Konica Minolta, Osaka, Japan). The colour values of the fresh and dried samples were expressed as L^* (whiteness/darkness), a^* (redness/greenness), and b^* (yellowness/blueness). The total colour difference (ΔE) between samples was calculated according Eq. (7):

$$\Delta E = \sqrt{\left(L_0^* - L^*\right)^2 + \left(a_0^* - a^*\right)^2 + \left(b_0^* - b^*\right)^2} \quad (7)$$

Subscript 0 refers to the colour of the fresh sample. The parameters of *Chroma* C^* (color saturation) and *Hue* angle h^* (color tone) were calculated according to Eq. (8) and (9):

$$C^* = \sqrt{a^{*2} + b^{*2}} \quad (8)$$

$$h^* = tan^{-1}\left(\frac{b^*}{a}\right) \quad (9)$$

Also, the browning index (BI) weas calculated according to Maskan (2001) using Eq. (10) and (11):

$$BI = 100 \times \left(\frac{X - 0.31}{0.17}\right) \quad (10)$$

where

$$X = \frac{a^* + 1.75 \bullet L}{5.645 \bullet L^* + a^* - 3.012 \bullet b^*} \quad (11)$$

2.12. UHPLC analysis

The powders obtained at 45 °C were selected for further investigation. Both powders were extracted using an ethanol:glacial acetic acid mixture (ratio 9:1, *v/v*) (solid–liquid ratio 1:10, *w/v*). The solid–liquid mixtures were extracted using a sonication water bath at 30 °C for 30 min, followed by centrifugation at 6000 rpm for 10 min at 4 °C. The supernatants were collected, and the extraction was repeated three times. The collected supernatants were concentrated to dryness under reduced pressure at 40 °C (AVC 2–18, Christ, UK). The chromatographic analysis was performed with a Thermo Scientific equipment that was coupled with a Thermo Scientific Dionex Ultimate 3000 Series RS pump, Thermo Scientific Dionex Ultimate 3000 Series TCC-3000 RS column compartments and a Thermo Fisher Scientific Ultimate 3000 Series WPS-3000RS autosampler. The whole equipment was controlled by the 7.2 version of Chromeleon Software (Thermo Fisher Scientific, Waltham, MA and Dionex Softron GMbH Part of Thermo Fisher Scientific, Germany). For the separation method, a 35 min linear gradient was applied on an Accucore U-HPLC Column C18 (150 X 2.1 mm, 2.6 μm), (Thermo Fisher Scientific, Germany). The mobile phase consisted of two phases A, acidified ultrapure water (acidified with formic acid at a ratio of 500 μL/L until pH 2.5), and B, pure methanol. The steps of the gradient were as follows: 0–1 min 100% A, 1–10 min linear increase to 30% B, 10–26 linear increased to 100% B and held for 4.0 min, 30–32.5 decreasing to 0% B. The column's temperature was 40 °C while the equilibration time to reach the prior conditions was 2.5 min. The flow rate was established at 0.4 mL/min. For the MS parameters, a HESI (Heated Electrospray) ionisation source was used, while the parameters were optimised in terms of the nitrogen as the auxiliary gas that had a flow rate at 8 and 6 units, respectively. The temperature value of 300 °C was set for the auxiliary gas heater, the source heater, and the capillary. The S lens RF level was 50 while the electrospray voltage was 2800 V. The targeted compounds were identified and detected using a Q-Exactive mass spectrometer. The scan was performed in a negative mode, at the resolving power of 70,000 FWHM, at *m/z* 200, with a *m/z* scan range between 100 and 1000 Da. The injection time was set at 200 ms, with the scan rate being at 2 scans/*sec* while the automatic gain control (AGC) was set at $3e^6$. The calibration was performed in both ways, positive and negative modes. One full scan event was associated to six scan events, under the previously mentioned parameters and five MS-MS events were done. In the MS^2 scan, the *m/z* precursor ion ranged between 95 and 205, 195–305, 295–405, 395–505, and 500–10005, while being selected consecutively and fragmented within a HCD higher-energy collisional dissociation cell. The obtained ions were measured, at a resolving power of 35,000 FWHM, in five separate Orbitrap scans. The collision energy was normalised for the fragmentation events, and it was performed at 30, 60, and 80 NCE. The C-trap parameters were an automatic Gain Control (AGC) target of $1e^6$ with the injection time of 100 ms. To evaluate the obtained data, the Quan/Qual Browser Xcalibur 2.3 software (Thermo Fisher, Germany) was used. The mass tolerance was set at 5 ppm for both of the analysis modes. The MS/MS analysis took into consideration the detection of at least two fragment ions that had the appropriate ion-ratio when compared to the ratio of the available

reference standards. Nonetheless, for the compounds for which no standard was available, the chemical Chemspider database (www.chemspider.com) was searched to find the most reasonable molecular formula with the lowest mass error. As it is well-known, polyphenols derive from the same chemical skeleton structure, so that NORMAN MassBank (https://massbank.eu/MassBank/), mzCloude™ Advanced Mass Spectral Database (https://www.mzcloud.org/), and PubChem (https://pubchem.ncbi.nlm.nih.gov/) were utilized to further confirm the chemical structure. To generate the presumptive fragmentation pattern of the targeted compounds, ACDLabs MS Fragmenter 2019.2.1 software was used for a comparison analysis.

2.13. Hyperspectral dark-field microscopy

Hyperspectral dark-field microscopy (HDFM) analysis was carried out using the CytoViva Hyperspectral Imaging System (CytoViva Inc., USA). Dark-field hyperspectral images (DF-HSI) and hyperspectral profile were obtained using 60× objective lenses of the microscope system (BX51, Olympus, USA) equipped with a 150 W halogen light source (Fiber-Lite, Dolan-Jenner, USA) and a hyperspectral camera (CytoViva hyperspectral imaging system 1.4. DF-HSI were processed by ENVI data analysis software (ENVI 4.8).

2.14. Inhibitory effect of bioactive on α-amylase on fluorescence emission spectra basis

The fluorescence emission spectra were recorded with a LS-55 Luminescence Spectrometer (Perkin Elmer, Waltham, MA, USA), using a 1.0 cm quartz cell and a thermostat bath, which allowed the maintenance of a constant temperature of 25 ± 0.1 °C during scanning. The excitation and emission width of slits was set at 10.0 nm. The emission spectrum were recorded at λ_{ex} of 290 nm and λ_{em} ranging from 320 to 420 nm, whereas the intensity recorded at the maximum emission wavelength (λ_{max}) was used to calculate the binding constants. In all the experiments, the florescence intensity values were corrected for dilution effects, by substracting the intensity of the anthocyanins extract in buffer. The investigations consisted in analysing the α-amylase conformational changes induced by successive titration with increasing concentrations of the both extracts. Therefore, 0.2 mL of α-amylase (5 mg/mL in phosphate buffered saline (PBS), pH 7.4) were placed into the quartz cuvette containing 2.50 mL of phosphate buffer (pH 7.4) followed by addition of extract (at concentration ranging from 0 to 9.13 μMol C3G/mL for CD extract and from 0 to 14.21 μMol C3G/mL for IR extract, on cyanidin-3-*O*-glycoside basis). The binding constants (K) and the number of binding sites (n) were calculated, considering the equilibrium between free and bound molecules given by the binding of small molecules of inhibitors to equivalent sites on a macromolecule (Zhou et al. 2017):

$$\frac{F_0}{F_0 - F} = \frac{1}{n} + \frac{1}{K} \times \frac{1}{[TAC]} \tag{12}$$

where F_0 and F are the relative fluorescence intensity of α-amylase in the absence and presence of the extract, respectively. [TAC] is the concentration of total monomeric anthocyanins.

2.15. The thermodynamic parameters for α-amylase-anthocyanins binding

In order to estimate the thermodynamic parameters, 0.25 mL of α-amylase solutions was subjected to thermal treatment at temperatures ranging from 25 to 90 °C for 15 min. The heating time was selected such as to ensure the irreversibility of the conformational changes. The thermodynamic parameters were calculated at different temperatures using the van't Hoff equation:

$$lnk = -\frac{\Delta H}{RT} + \frac{\Delta S}{R} \tag{13}$$

where K is the binding constant at the corresponding temperature based on equation (13), T is the experimental temperature, R is the gas constant. ΔH and ΔS are enthalpy and entropy change and were derived from the slope and intercept of the regression line obtained by plotting the natural logarithm of K versus $1/T$. Gibbs free energy (ΔG) of the reaction was calculated using the equation:

$$\Delta G = \Delta H - T \times \Delta S \tag{14}$$

2.16. α-amylase inhibitory effect of the extracts

In order to calculate the inhibitory effect of the extracts on α-amylase activity, serial dilutions of the extracts, ranging from 0 to 9.13 μMol C3G/mL for CD extract and 14.21 μMol C3G/mL for IR extract were added to test tube and 100 μL of α-amylase solution (5 mg/mL in 0.1 M PBS, pH 7.4) and allowed to incubate at 25 °C for 20 min. Further, in each test tube, 100 μL of 1% soluble starch solution dissolved in PBS and previously boiled for 5 min was added and incubated for another 20 min at 37 °C. Finally, 200 μL mL of dinitro salicylic acid reagent was added and the mixtures were heated at 100 °C for 5 min in a water bath. Further, the samples were diluted with 2 mL of distilled water and absorbance read at wavelength of 540 nm. The enzyme inhibition was calculated using equation (15):

$$Inhibitory\ effect\ (\%) = \frac{A_0 - A_s}{A_0} x100 \tag{15}$$

The inhibitory concentration (IC_{50}) was estimated from the slope of the regression line obtained by plotting the natural inhibitory effect versus anthocyanins concentration.

2.17. Statistical analysis

All the experiments were performed in triplicates. The values are reported on a dry basis and presented as mean ± standard error. Statistically significant differences among the results were analyzed by one-way analysis of variance (ANOVA), followed by the Tukey test at a significance level of 5% ($p < 0.05$). The statistical software package Minitab version 19 (Romsym Data, Bucharest, Romania) was used for the analysis.

3. Results and discussion

3.1. Analysis of drying curves and mathematical modelling

The drying temperature and time play an important role in the quality of dried fruits and vegetables. In general, using low temperature for drying will activate the enzymatic browning process of fruits and vegetables, whereas in case of a higher temperature, the most important nutrients and secondary metabolites will degrade. Therefore, in order to preserve the biological potential of the material, it is essential to choose the most suitable temperatures for drying. In our study, variations of moisture ratio versus drying time during drying are shown in Fig. 1 (A). For both drying methods, as expected, the increase of drying temperature decreased the time for GP purée water removal, which led to the reduction of drying time. As it can be observed from Fig. 1, the moisture ratio (MR), decreases linearly with time, until the point of critical moisture content is reached. This point represents the average material moisture content where the drying rate begins to decrease. This period is continued with a non-linear decrease of moisture ratio with time, until the solid (GP purée) achieves the equilibrium moisture content (M_e), and drying stops. The drying times at different air temperature of 40 °C, 45 °C and 50 °C were found to be 270 min, 240 min and 210 min in the case of CD, while for IR drying these values corresponded to 240 min,

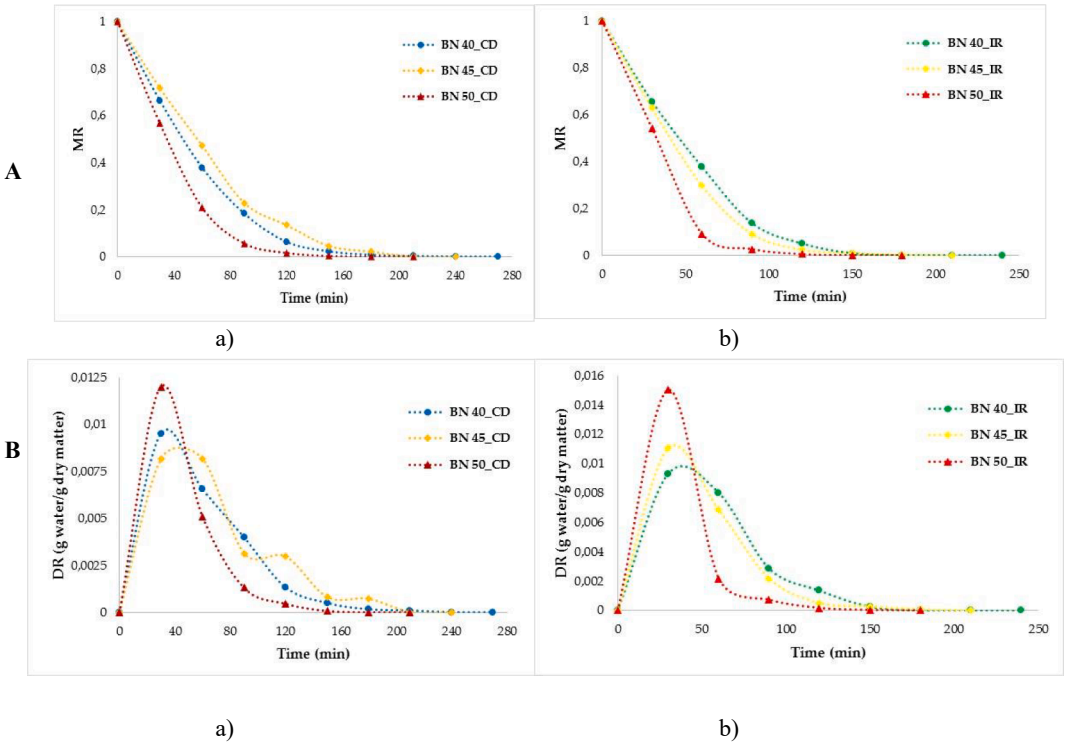

Fig. 1. Variations of moisture content (A) and drying rate (B) with drying time: a) convective drying method, b) IR drying method.

210 min and 180 min, respectively. Compared to CD, the drying time for IR method decreased with 11% at 40 °C, 12.5% at 45 °C and with 14.3% at 50 °C. This correlation was also observed by Ross et al. (2020) and Cascaes Teles et al. (2018), who studied the drying process of GP from Merlot and Pinot Noir, respectively, at similar temperatures.

The variation of drying rate with drying time are shown in Fig. 1 (B). From Fig. 1 (B) it can be observed that the drying process takes place in two stages. In the first stage, the drying rate reaches its maximum values for both drying methods after 30 min (0.0081 – 0.0119 g water/g DW for CD and 0.0093 – 0.015 g water/g DW for IR), probably due to the high moisture content and due to drying on the surface of GP purée. The second stage drying process takes place with the decrease of moisture content in the GP purée samples. The drying rate values range between 0.00071 and 0.00016 g water/g DW for CD and 0.000068 – 0.000023 g water/g DW for IR drying. This could be explained by a reduction in porosity of the purée samples due to a larger shrinkage, thus increasing the strength of water molecules movement, leading to further decrease in drying rates. Our results are in good agreement with those suggested by Darici & Şen (2015) for the convective drying of the kiwi fruits. The results achieved from the mathematical modelling at different drying methods and temperatures, as well as the parameters (R^2 and *SSR*), are presented in Table 2 (Supplementary material). For all models, the coefficient of determination (R^2) values were higher than 0.95, while the sum of the residual squares (SSR) values were under 0.4. Page model showed the highest R^2 values (0.990 to 0.999) and lowest SSR values (0.00029 to 0.030) than other models for all drying temperatures for both drying methods. For this model, the calculated drying constant (k) values ranged from 0.188 to 0.404 s^{-1} while the n values ranged from 0.397 to 1.558 and were affected by drying methods and temperatures. Similar results were obtained for other biological material such as fermented Merlot grape pomace (Ross et al., 2020) and Pinot Noir grape pomace (Cascaes Teles et al., 2018) which found the Page model best described for experimental data of drying grape pomace.

3.2. D_{eff} and E_a

The effective moisture diffusivity (D_{eff}) and activation energy (E_a) values of GP purée are shown in Table 1. The D_{eff} was described using the experimental drying data, by plotting experimental drying data in terms of ln*(MR)* versus drying time (t), as described in Eq. (3). The D_{eff} values increased with increasing temperature from 40 to 50 °C ($p \leq 0.05$), in good agreement with the results reported by Ross et al. (2020). The D_{eff} value ranged from 6.64×10^{-9} to 9.38×10^{-9} m^2/s for CD and from 8.83×10^{-9} to 11.16×10^{-9} m^2/s for IR, being positively correlated with the drying temperatures. According to Lemus-Mondaca et al. (2021), different factors such as moisture distribution in the samples, pomace type, load density, drying temperature, shrinkage of raw material, and drying environment could influence the D_{eff} values. In this study, the D_{eff} values of GP purée are within the general ranges mentioned in the literature (10^{-12} to 10^{-8} m^2/s) for biological materials

Table 1
Effective moisture coefficient and activation energy of GP purée as affected by temperature.

Sample code*	Drying method	t, (°C)	$D_{eff} \times 10^{-9}$ (m^2/s)	R^2	E_a (kJ/mol)	R^2 (E_a assessment)
BN 40_CD	*Convective drying*	40	6.64	0.9796	29.366	0.9215
BN 45_CD		45	7.26	0.9715		
BN 50_CD		50	9.38	0.9680		
BN 40_IR	*IR drying*	40	8.83	0.9161	19.391	0.9735
BN 45_IR		45	10.25	0.9793		
BN 50_IR		50	11.16	0.9822		

*BN_{CD} - GP purée dried by convection method, BN_{IR}—GP purée dried by infrared (IR) method. Means that do not share a letter as a superscript (A, B, C) are significantly different.

(Zogzas et al., 1996). Similar results were obtained for carrot pomace dried through CD (Kumar et al., 2012) and for apricot pomace dried with IR radiation (Kayran & Doymaz, 2019).

The activation energy (E_a) values, estimated by the Arrhenius equation, was 29.366 kJ/mol for CD and 19.391 kJ/mol for IR. It has beed reported that the E_a value for drying of different food materials range between 12.7 and 110 kJ/mol (Zogzas et al., 1996). The E_a value depends on the basic properties of the material, ripening degree, texture composition and surface area (Li et al., 2015). Results reported for drying of by-products include 23.05 kJ/mol for carrot pomace (Kumar et al., 2012), 39.66 kJ/mol for pomegranate peel (Kara & Doymaz, 2015) and 25.41 kJ/mol for grape marc (Doymaz, 2019).

3.3. Cell viability

Probiotic products are becoming increasingly popular, especially non-dairy strains. In our study, the GP purées were inoculated with an *L. casei* 431® inoculum at a level of 9.1 log CFU/g. The viable cells were determined after 14 days of storage at 4 °C, during which a 2 log decrease in CFU/g up to 7.07 log CFU/g and 7.37 log CFU/g for CD and IR drying were found. The decrease in viable cells was observed in all dried GP samples, possibly due to the drying temperature and water content. Although there was a minor reduction in *Lactobacillus* viability in all dried samples at the beginning of the storage period, an intense decrease in viability was discovered at the end of the storage period. The reduction was limited for the conventional treatment at 40 °C. Fermented fruit and vegetable pomace has been studied as a dietary component in the past, but only a few attempts have been made to assess the lactic acid bacteria content after drying (Janiszewska-Turak et al., 2021). Ribeiro et al. (2014) studied the kinetics of kiwi and strawberry pieces dried at 40 °C when incorporating *Lactobacillus plantarum* and reported 0.5–1.5 log decrease after 37 days of storage at 4 °C. The use of pomace as a silage additive resulted in good quality silage, regardless of the use of additional lactic acid bacteria (Bureenok et al., 2019). In order to have a powder with probiotic properties, it is mandatory to maintain a minimum 6 log of viable cells at the end of storage time. From our results, the maximum storage time may be extended to 20 days at 4 °C.

3.4. Bioactive compounds and antioxidant activity in fresh and dried GP purée

The bioactive compounds and antioxidant activity for GP purée dried under different conditions are presented in Table 2. From Table 2 it can be observed that all the bioactive content increase by drying, due to reducing the water content. However, the extractibility of polyphenols, flavonoids and anthocyanins increased up to 45 °C. As expected, at higher temperature, the polyphenolic content decreased, thus impacting the antioxidant activity. The highest polyphenolic contents, in terms of TPC, TFC and TAC were obtain by IR drying at 45 °C. During drying, the breakdown of ester linkage among phenolic moieties and cell walls causes the increase of free phenolics in the tissue matrix (Ping et al., 2019). The increase of TFC may be due to some new formed compounds produced after thermal decomposition, such as 2,4,6-trihydroxybenzoic acid from quercetin and protocatechuic acid from rutin (Chaaban et al., 2017). At higher temperature, up to 50 °C, the polyphenolic contents decreases, due to the presence of heat-sensitive, unstable and easily deteriorated compounds. The frequent degradation reactions are enzymatic oxidation of phenolic compounds, due to moisture, oxygen and deteriorative enzymes (Ping et al., 2019). Our results are in good agreement with those reported by Sui et al. (2014) using both CD and IR drying of wine grape pomace.

Table 2
Bioactive compounds and antioxidant activity of fresh and dried GP puree.

Drying method/ Sample code	Antioxidant activity, mMol TE/g DW	TPC, mg GAE/g DW	TFC, mg EC/g DW	TAC, mg C3G/g DW
Fresh GP purée				
BN_0	63.26 ± 1.23^{A}	9.16 ± 0.13^{A}	14.83 ± 0.14^{A}	0.72 ± 0.15^{B}
Convective drying				
BN 40_CD	17.27 ± 0.17^{A}	21.69 ± 0.19^{A}	16.47 ± 0.27^{A}	1.07 ± 0.59^{B}
BN 45_CD	18.55 ± 0.21^{A}	22.35 ± 0.13^{A}	29.80 ± 0.25^{A}	1.49 ± 0.08^{B}
BN 50_CD	17.09 ± 0.11^{A}	20.76 ± 0.15^{A}	22.17 ± 0.15^{A}	0.84 ± 0.01^{B}
IR drying				
BN 40_IR	18.87 ± 0.18^{A}	16.99 ± 0.18^{A}	24.73 ± 0.17^{A}	1.10 ± 0.07^{B}
BN 45_IR	20.07 ± 0.15^{A}	26.21 ± 0.12^{A}	33.03 ± 0.31^{A}	1.78 ± 0.08^{B}
BN 50_IR	18.63 ± 0.32^{A}	17.93 ± 0.14^{A}	31.83 ± 0.28^{A}	0.94 ± 0.09^{B}

*BN_0-fresh GP purée sample, BN_{CD}-GP purée dried by convection method, BN_{IR}-GP purée dried by infrared (IR) method. Means that do not share the same letter as a superscript (A, B, C) are significantly different.

3.5. Colour of fresh and dried GP purée

Color parameters of L^* (whiteness/darkness), a^* (redness/greenness), and b^* (yellowness/blueness) of GP purée, fresh and dried were studied (Table 3, Supplementary material). The lightness (L^*) value reduced with the increase of drying temperature for both drying methods, whereas no significant differences between the color of fresh and dried samples were found. This could be related to the increase of browning index (BI) value that was associated with Maillard reaction (enzyme-free browning process). This reaction imply brown pigment synthesis through GP interactivity between sugars and proteins (Somjai et al., 2022). The a^* and b^* values of GP dried samples representing redness/greenness and yellowness/blueness, respectively, were lower compared with the fresh sample. This may occur due to the degradation of anthocyanins during drying process. As can be seen, the a^* and b^* values for the dried samples increased with temperature. Total color difference ΔE values were estimated relative to raw GP purée. After drying, the ΔE values for all samples increased and were less than 12, which represents the reference value according to Zhang et al. (2016). The total color change of the dried GP purée samples varied from 6.26 ± 0.47 to 6.97 ± 0.56 units, being influenced by time, temperature and drying method. The colour tone (h^*) (Table 3, Supplementary material) values increased for all dried samples compared to raw GP purée. The C^* values slightly decreased after drying. The colour saturation values varied between the dried samples and the model was comparable to the b^* color coordinate. An important indicator for browning reaction is browning index (BI), described as brown color purity (Bathula et al., 2020). For both drying methods the values of BI increased, due to the enzymatic reactions.

3.6. Phytochemical profile of the selected powders

Based on the above-mentioned results, the powders dried at 45 °C were selected for further investigations. The powders were subjected to repeated extractions, leading to an increase in TAC from 1.49 ± 0.08 mg C3G/g DW to 12.19 ± 0.21 mg C3G/g DW in CD powder and from 1.78 ± 0.08 mg C3G/g DW to 7.82 ± 0.24 mg C3G/g DW in IR powder. No significant increase in flavonoids content due to the repeated extraction was observed, while the content of TPC increased significantly, about 1.8 times in the samples dried by CD (40.74 ± 0.72 mg GAE/g DW) and 1.6 times in those dried by IR (42.06 ± 0.34 mg GAE/g DW). The TAC and TPC increase lead to higher antioxidant activity of the extracts (66.73 ± 0.71 mMol Trolox/g DW and 67.81 ± 0.59 mMol Trolox/g DW, respectively).

Both of the powders were analysed by UHPLC, with the main components being identified and quantified. Table 3 shows the obtained

Table 3
Presumptive identification of extractable polyphenols from dried grape marc powders, determined by UHPLC-MS analysis.

Compound	Formula	Theoretical *m/z*	Convective drying	Infrared drying
			µg/mL extract	
FLAVONOLS				
Syringetin *O*-di-hexoside	$C_{29}H_{34}O_{18}$	669.16724	8.57 ± 0.65	8.59 ± 0.23
Myricetin *O*-di-hexoside	$C_{27}H_{30}O_{18}$	641.13594	11.04 ± 0.88	11.24 ± 0.45
Myricetin hexoside-glucuronide	$C_{27}H_{28}O_{19}$	655.11523	10.81 ± 0.23	10.80 ± 0.33
Myricetin 3-*O*-galactoside	$C_{21}H_{20}O_{13}$	479.08314	13.74 ± 0.11	13.75 ± 0.56
Myricetin 3-O-glucuronide	$C_{21}H_{18}O_{14}$	493.06240	10.20 ± 0.45	10.18 ± 0.99
Myricetin 3-O-glucoside	$C_{21}H_{20}O_{13}$	479.08314	13.74 ± 0.98	13.75 ± 0.34
Dihydroquercetin 3-*O*-hexoside	$C_{21}H_{22}O_{12}$	465.10387	9.84 ± 0.79	9.82 ± 0.33
Rutin	$C_{27}H_{30}O_{16}$	609.14613	26.31 ± 0.65	26.35 ± 0.42
Quercetin 3-*O*-galactoside/glucoside	$C_{21}H_{20}O_{12}$	463.08822	12.29 ± 0.23	12.30 ± 0.45
Quercetin 3-*O*-glucuronide	$C_{21}H_{18}O_{13}$	477.06749	12.05 ± 0.56	12.03 ± 0.66
Laricitrin 3-O-hexoside	$C_{22}H_{22}O_{13}$	493.09879	12.49 ± 0.65	12.50 ± 0.12
Laricitrin 3-*O*-glucuronide	$C_{22}H_{20}O_{14}$	507.07805	12.48 ± 0.99	12.49 ± 0.45
Kaempferol *O*-rhamnosyl-hexoside	$C_{27}H_{30}O_{15}$	593.15122	13.62 ± 0.25	13.61 ± 0.04
Dihydroquercetin 3-*O*-rhamnoside	$C_{21}H_{22}O_{11}$	449.10896	8.03 ± 0.22	8.02 ± 0.68
Isorhamnetin *O*-rhamnosyl-hexoside	$C_{28}H_{32}O_{16}$	623.16178	13.80 ± 0.09	13.79 ± 0.11
Kaempferol 3-*O*-galactoside	$C_{21}H_{20}O_{11}$	447.09331	13.55 ± 0.55	13.54 ± 0.12
Syringetin 3-*O*-galactoside/glucoside	$C_{23}H_{24}O_{13}$	507.11441	13.69 ± 0.58	13.12 ± 0.57
Kaempferol 3-*O*-glucoside	$C_{21}H_{20}O_{11}$	447.09328	13.43 ± 0.87	13.55 ± 0.21
Kaempferol 3-*O*-glucuronide	$C_{21}H_{18}O_{12}$	461.07257	13.39 ± 0.07	13.40 ± 0.29
Isorhamnetin 3-*O*-glucuronide	$C_{22}H_{20}O_{13}$	491.08314	13.75 ± 0.11	13.74 ± 0.08
ANTHOCYANINS				
Cyanidin −3,5-*O*-diglucoside	$C_{28}H_{33}O_{17}$	640.16450	6.03 ± 0.34	not determined
Cyanidin-3-*O*-monoglucoside	$C_{21}H_{21}O_{11}$	448.10113	9.60 ± 1.22	9.62 ± 0.98
Malvidin-3-*O*-monoglucoside	$C_{23}H_{25}O_{12}$	492.12735	0.67 ± 0.01	0.66 ± 0.01
STILBENS				
Z-Piceid	$C_{20}H_{21}O_8$	388.11639	not determined	9.54 ± 0.34
Pallidol-3-O-glucoside	$C_{34}H_{31}O_{11}$	614.17938	not determined	6.14 ± 0.22
Dimer 2	$C_{28}H_{21}O_6$	452.12656	5.79 ± 0.67	5.79 ± 0.45
trans-Resveratrol	$C_{14}H_{11}O_3$	226.06357	13.96 ± 0.33	6.17 ± 0.32
FLAVONOIDS AND PHENOLIC ACIDS				
Epicatechin	$C_{15}H_{14}O_6$	289.07176	110.20 ± 4.54	132.95 ± 2.11
Catechin	$C_{15}H_{14}O_6$	289.07176	248.52 ± 3.21	289.53 ± 2.98
p-Coumaric acid	$C_9H_8O_3$	163.03954	18.26 ± 0.98	20.65 ± 3.56
Syringic acid	$C_9H_{10}O_5$	197.04555	33.49 ± 1.23	32.54 ± 1.01
Glycitein	$C_{16}H_{12}O_5$	283.06122	10.22 ± 1.01	9.11 ± 0.99
Chlorogenic acid	$C_{16}H_{18}O_9$	353.08783	6.84 ± 0.54	2.81 ± 0.08
Hyperoside (quercetin 3-galactoside)	$C_{21}H_{20}O_{12}$	463.08768	4475.44 ± 5.68	4730.66 ± 7.98
Apigenin	$C_{15}H_{10}O_5$	269.04502	2.36 ± 0.56	2.40 ± 0.31
Gallic acid	$C_7H_6O_5$	169.01427	407.30 ± 5.68	424.99 ± 2.34
Pinocembrin	$C_{15}H_{12}O_4$	255.06631	104.57 ± 2.11	105.74 ± 2.11
Galangin	$C_{15}H_{10}O_5$	269.04557	477.70 ± 5.43	609.51 ± 8.90
Chrysin	$C_{15}H_{10}O_4$	253.05066	5.49 ± 0.47	5.30 ± 0.45
Kaempferol	$C_{15}H_{10}O_6$	285.04049	35.60 ± 0.99	38.76 ± 2.89
Naringin	$C_{27}H_{32}O_{14}$	579.17185	27473.95 ± 123.87	34880.94 ± 6.78
Naringenin	$C_{15}H_{12}O_5$	271.06122	1.31 ± 0.04	0.86 ± 0.09
Quercetin	$C_{15}H_{10}O_7$	301.0354	1590.05 ± 4.57	1635.86 ± 4.53
Abscisic acid	$C_{15}H_{20}O_4$	263.12891	16.20 ± 1.23	19.02 ± 1.11
Isorhamnetin	$C_{16}H_{12}O_7$	315.05105	14.06 ± 1.01	14.89 ± 1.01
Daidzein	$C_{21}H_{20}O_9$	415.10348	4.92 ± 0.22	4.72 ± 0.98
Myricetin	$C_{15}H_{10}O_8$	317.03032	119.66 ± 3.21	105.86 ± 2.34

Results are expressed as mean ± standard deviation (n = 2).

fragmentation patterns for each polyphenol that was analysed. During the extraction, anthocyanins are released from the cellular walls and are prone to form binding interactions to create some other structural patterns and thus different compounds. Regarding their chemical structure, the acylated forms have shown a higher binding rate with 18.5% more than the non-acylated forms. The total anthocyanin content was higher for the CD powder (16.49 µg/mL extract) compared to the IR powder (10.32 µg/mL extract). Probably, the lower concentration appears because of a lower extractability rate of these compounds in the IR powder. The presumptive identification of the anthocyanins highlighted the presence of 28 anthocyanins and their corresponding derivatives. In both samples, the main anthocyanin found was cyanidin-3-*O*-monoglucoside with a concentration of 9.80 ± 1.22 µg/mL extract for the CD powder and 9.62 ± 0.98 µg/mL extract for the IR powder. The concentration of the other two anthocyanins, cyanidin-3,5-*O*-diglucoside and malvidin-3-*O*-monoglucoside, were rather similar when comparing the two powders. Traces of petunidin-3,5-*O*-diglucoside, delphinidin-3-*O*-monoglucoside, peonidin-3,5-*O*-diglucoside, delphinidin acetyldiglucoside, malvidin-3,5-*O*-diglucoside, petunidin-3-*O*-monoglucoside, peonidin-3-*O*-monoglucoside, delphinidin-3-*O*-acetylmonoglucoside, petunidin caffeoyl diglucoside, delphinidin p-coumaroyldiglucoside, petunidin-3-*O*-acetylmonoglucoside, delphinidin-3-*O*-caffeoylmonoglucoside, petunidin p-coumaryldiglucoside, cyanidin p-coumaryldiglucoside, malvidin-3-*O*-acetylmonoglucoside, peonidin-3-*O*-acetylmonoglucoside, petunidin-3-*O*-caffeoylmonoglucoside, malvidin p-coumaryldiglucoside, delphinidin-3-*O*-p-coumarylmonoglucoside, peonidin p-coumaryldiglucoside, malvidin-3-*O*-caffeoylmonoglucoside, cyanidin-3-*O*-p-coumarylmonoglucoside, petunidin-3-*O*-p-coumarylmonoglucoside, malvidin-3-*O*-p-coumarylmonoglucoside, peonidin-3-*O*-p-coumarylmonoglucoside were also found. The flavonols profile revealed a higher concentration in the CD powder (270.96 µg/mL extract) when compared to IR powder (256.37 µg/mL extract), the major compound being rutin (the glycoside combining the flavonol quercetin and the

disaccharide rutinose) with a concentration of 26.31 ± 0.65 μg/mL extract for the CD powder and 26.35 ± 0.42 μg/mL extract for the IR powder. Trans-resveratrol was found in a concentration of 13.96 ± 0.33 μg/mL extract for the CD powder and 6.17 ± 0.32 μg/mL extract for the IR powder. Other compounds included isorhamnetin *O*-rhamnosyl-hexoside, followed by myricetin 3-*O*-galactoside and myricetin 3-*O*-glucoside, and kaempferol *O*-rhamnosyl-hexoside, kaempferol 3-*O*-galactoside, syringetin 3-*O*-galactoside/glucoside, kaempferol 3-*O*-glucoside and kaempferol 3-*O*-glucuronide. Different flavonoids and phenolic acids were also detected, with a significantly higher concentration in the IR powder, of 43.10 μg/mL extract, when compared to 35.18 μg/mL extract in the CD powder. In terms of flavonoids, the main compounds were quercetin 3-galactoside, naringin and quercetin, the second being the major compound for this class with a concentration of 27473.95 ± 123.87 μg/mL extract for the CD powder and 34880.94 ± 6.78 μg/mL extract for the IR powder. In the group of phenolic acids, the major compound was represented by gallic acid with a content of 407.30 ± 5.68 μg/mL extract for the CD powder and 424.99 ± 2.34 μg/mL extract for the IR powder. The stilbenes concentration varied also amongst the two powders, so that the IR powder displayed a higher content of 27.64 μg/mL extract when compared to the CD powder of 19.75 μg/mL extract. Characteristic compounds such as caraphenol B, Z – Ɛ- viniferin, E– Ɛ- viniferin, Z-miyabenol C, E-miyabenol C were also traced in both of the powders. Flamini et al. (2015) studied also the grape polyphenols by UHPLC/QTOF. The authors have performed several analyses on grape metabolomics and have unidentified a large number of grape and wine metabolites. Amongst flavonols, several compounds were identified such as kaempferol, quercetin, myricetin, isorhamnetin, laricitrin, syringetin, and dihydroflavonol, while in terms of anthocyanins, pelargonidin-3-*O*-glucoside, cyanidin-3-*O*-glucoside, peonidin-3-*O*-glucoside, delphinidin-3-*O*-glucoside, petunidin-3-*O*-glucoside, malvidin-3-*O*-glucoside, and anthocyanidin-3,5-*O*-diglucoside were detected.

3.7. Spectral analysis of the selected powders

In Fig. 2, the microscopic details of both powders highlighted the homogeneity of the IR sample (Fig. 2, b) compared to that obtained by CD. In CD sample (Fig. 2, a), the aggregations of bioactive in clusters of variable sizes and shapes can be observed. Instead, in the IR sample, lactic acid bacteria can be clearly distinguished (Fig. 2, b). The mean spectral comparison of CD samples vs. IR is captured in Fig. 2 (c). A distinct and consistent 25 nm peak shift is observed across these two samples (from 700 nm to 725 nm, respectively). Additionally, the CD sample has a more distinct peak shoulder at 625 nm. At a higher drying temperature (CD), probably the faster dehydration, the denaturation of some enzymes caused a partial degradation of the bioactive with the formation of derivatives that generated this peak shift and the appearance of the new peak shoulder compared to the variant obtained by IR (Chaaban et al., 2017; Ping et al., 2019; Sui et al., 2014).

3.8. Changes in conformation and fluorescence emission spectra of α-amylase

This approach exploits the fluorescence of tryptophan residues in proteins, due to its sensitivity to the polarity of its local environment (Vivian & Callis). The fluorescence emission spectra of α-amylase at two temperatures (25 °C and 90 °C) treated with increased concentration of both extracts are shown in Fig. 3. With the gradual addition of dried GP extracts, the fluorescence intensity of α-amylase gradually decreased. Therefore, increasing the anthocyanins concentration from 0 to 9.13 μMol C3G/mL for CD extract and to 14.21 μMol C3G/mL for IR extracts, the relative fluorescence intensity gradually decreased from 100% to 23.7% for CD powder and to 19.8% for the IF powder, respectively (Fig. 3). The highest quenching effect of the IR extract is given by the highest TAC content. The λ_{max} significantly red-shifted with increasing the anthocyanins concentration, for both extracts. Therefore, in case of

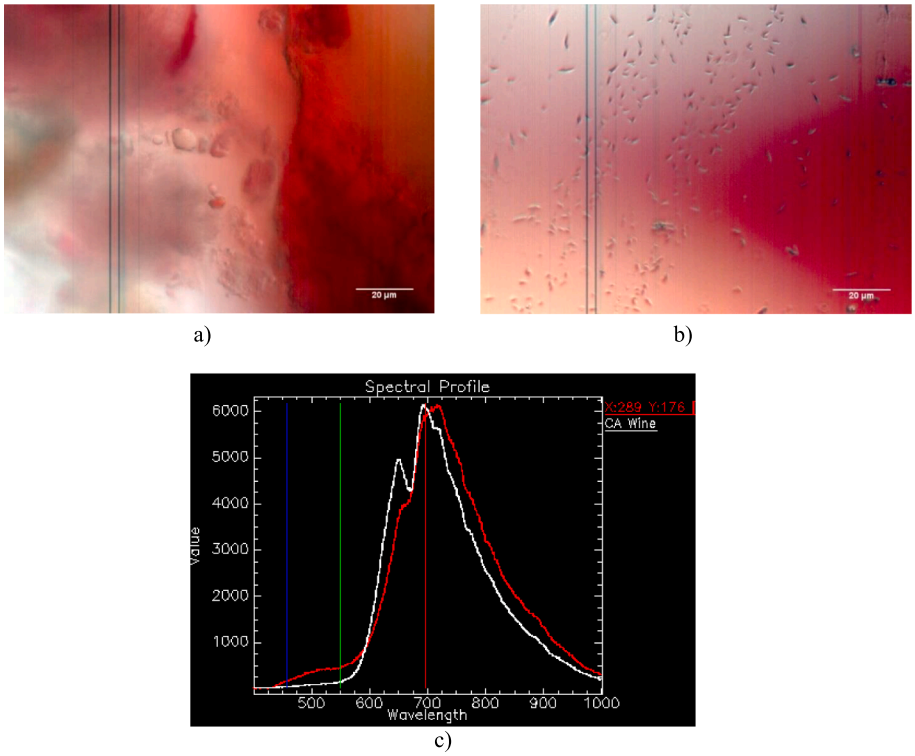

Fig. 2. Dark-field hyperspectral images (DF-HSI) of the convective (a) and infrared dried powders (b), mapping of convective (white) vs. infrared (red) spectral profiles using CytoViva HSI optical microscopy (c). (For interpretation of the references to color in this figure legend, the reader is referred to the web version of this article.)

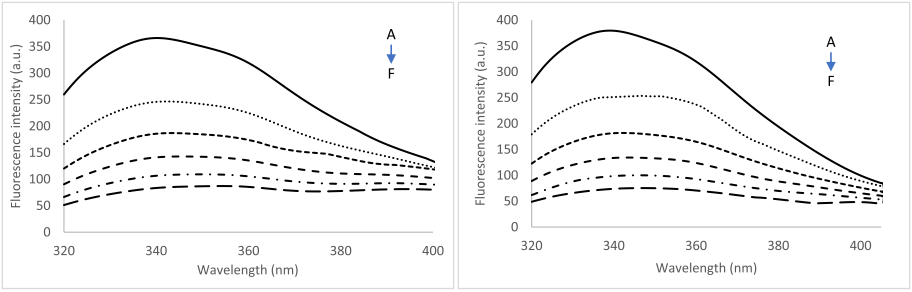

Fig. 3. Fluorescence emission spectra of α-amylase treated with convective (a) and infrared dried based extract (b) (α-amylase 5 mg/mL, antochyanins concentration ranged from 0 (A) to 9.13 μMol cyanidin-3-*O*-glucoside 9C3G)/mL (F) and to 14.21 μMol C3G/mL (F), respectively).

CD powder extract, the λ_{max} shifted from 340 nm in the absence of quencher to 354.5 nm in the presence of an anthocyanin's concentration of 9.13 μMol. The addition of IR extract generated 8 nm red-shift in λ_{max}, from 339 nm to 347 nm. These results highlighted the differentiated effect of the two extracts, due to the different moiety of different anthocyanins. In general, red-shifts in λ_{max} are associated with the extensive exposure of the previously buried Trp residues to the solvent molecules. Vivian & Callis (2001) explained that the extent of λ_{max} shifts is governed both by solvent and protein residues, with a higher contribution with increasing wavelength. The significant red-shifts arises from the shift in transition energy due to the change in dipole upon excitation. Heating caused unfolding of the enzyme conformation, up to 60 °C, when maximum red-shift of 18 nm was found. At higher temperatures, the polypeptide chains folds, with blue-shift of 3 nm, regardless the temperatures. When quenching, the maximum extent of red-shift was found only at 25 °C and 50 °C. When heating at temperatures higher than 50 °C, the successive titration with CD anthocyanins extracts lead to sequential blue-shifts, varying from 7.5 nm at 70 °C to 2 nm at 60 °C and 90 °C. The same trend was observed in the case of IR extracts, but to a lower extend. Therefore, at temperatures of 25 °C and 50 °C, significant red-shifts of 8 nm and 5 nm, respectively, were observed. At higher temperature, the maximum quenching effect was observed at temperatures of 70 °C and 90 °C, described by blue-shits of 6.5 nm. The binding constant (K) and the number of binding sites (n) are showed in Table 4 (Supplementary material). At 25 °C, the binding constant value were of $25.09 \pm 2.14 \times 10^{-2}$ Mol/L for CD extract and $15.94 \pm 1.61 \times 10^{-2}$ Mol/L for IR extract, respectively. The K values increased with increasing temperature up to 80 °C and slightly decreased at 90 °C. The increase–decrease of the K values may suggest a temperature mediated flexible fit between the enzyme and anthocyanins from the extracts. The binding constant values were significant different when considering the two types of extracts. This may be explained by the different anthocyanin's concentration in the extract and their moiety. The value of binding sites suggested that anthocyanins from the extracts had a single inhibition site or a single class of inhibition site on α-amylase. However, the K values for the CD extract were significantly higher when compared with the anthocyanins from IR powder (Table 4, Supplementary material). These differences may be explained by the different flexibility and mobility of the anthocyanins in the extract, which in turn is determined by the drying method. The thermodynamic parameters, in terms of changes in enthalpy were estimated at −60.47 kJ/Mol and −58.33 kJ/Mol for CD and IR extracts, respectively, whereas the changes in entropy showed similar values of 17.41 J/Mol/K and 16.46 J/Mol/K. The negative values of ΔH and positive for ΔS suggest that the major forces involved in protein–ligand interactions are hydrophobic forces. However, as explained by Ross & Subramanian (1981), it is possible that the binding between α-amylase and anthocyanins from the extracts to follow a two-step binding mode, involving a hydrophobic association and partial immobilization, followed by van der Waals interactions, leading to an inhibitory effect. Our results that both powder extracts interact with α-amylase, a protein with a particular pharmacological interest, suggesting that the anthocyanins from GP can act as antidiabetic molecules. Consequently, in order to estimate the inhibitory potential of both extracts on α-amylase, an *in vitro* assay was performed, using soluble starch solution (1%) dissolved in phosphate buffer as substrate. The IC_{50} values were 10.70 ± 0.12 μMol C3G/mL for the extract obtained from CD powder and 6.92 ± 0.09 μMol C3G/mL for the extract obtained from IR powder. The IC_{50} values were significant different than those obtained for acarbose (positive control) of 3.97 ± 0.62 mg/mL, highlighting the potential antidiabetic effect.

4. Conclusions

Due to is wide availability and lower economic value, red grape pomace shows interesting perspective in the field of the functional ingredients, foods and nutraceuticals. The added-value of red grape pomace is related with the wide bioactive profile. In this wotk, the effects of different drying methods on Băbească Neagră grape pomace purée inoculated with probiotic (*Lactobacillus casei ssp. paracasei (L. casei 431*®) were investigated, based on kinetic model and bacteria survival rate. The results showed that, whithin the temperature range of 40 °C and 50 °C, the temperature decreased the drying time and increased the drying rate. The infrared drying reduced the drying time, wich in turn allowed a better preservation of bioactive and lactic acid bacteria and colour. The effective diffusivity values were higher for infrared drying, leading to a lower activation energy. Both powders showed at least 7 log CFU/g DW. The powders dried at 45 °C were selected for spectral analysis, cromatographic advanced analysis and the inhibitory effect on metabolic syndrome associated α-amylase. The ultra-high liquid chromatography highlited a rich phenolic profile, with a wide range of anthocyanins, flavonols, stilbenes, and phenolic acids. The main anthocyanins were cyanidin-3,5-*O*-diglucoside and malvidin-3-*O*-monoglucoside, with concentration rather similar when comparing the two powders. A different spectral profile was observed, with a 25 nm red-shift in peak for infraded dried sample, probably due to the different moiety of bioactives. Based on fluorescence quenching, the anthocyanins induced significant conformational changes in α-amylase, driven by hydrophobic interactions. The IC_{50} values were significant higher for infrared powder, correlated with the higher content of bioactive. The results suggest that infrared drying method may be used to preserve the quality of Băbească Neagră GP purée. Further studies are currently developed in our laboratories, for selected powders properties, such as sorption isotherms, hygroscopicity, bulk and tapped density, particle density, and porosity.

CRediT authorship contribution statement

Larisa Anghel: Methodology, Validation, Writing – original draft. **Adelina Ștefania Milea:** Methodology, Validation, Writing – original draft. **Oana Emilia Constantin:** Methodology, Validation, Writing – original draft. **Vasilica Barbu:** Methodology, Validation, Writing – original draft. **Carmen Chițescu:** Methodology, Validation, Writing – original draft. **Elena Enachi:** Methodology, Validation, Writing – original draft. **Gabriela Râpeanu:** Methodology, Validation, Resources, Writing – original draft. **Gabriel – Dănuț Mocanu:** Conceptualization, Methodology, Software, Validation, Resources, Writing – original draft, Writing – review & editing, Project administration, Funding acquisition. **Nicoleta Stănciuc:** Conceptualization, Methodology, Software, Validation, Resources, Writing – original draft, Writing – review & editing, Supervision, Project administration, Funding acquisition.

Declaration of Competing Interest

The authors declare that they have no known competing financial interests or personal relationships that could have appeared to influence the work reported in this paper.

Data availability

Data will be made available on request.

Appendix A. Supplementary data

Supplementary data to this article can be found online at https://doi.org/10.1016/j.fochx.2023.100777.

References

Bathula, C., Kumar, K. A., Yadav, H., Ramesh, S., Shinde, S., Shrestha, N. K., et al. (2020). Ultrasonically driven green synthesis of palladium nanoparticles by Coleus Amboinicus for catalytic reduction and Suzuki-Miyaura reaction. *Colloids Surfaces B Biointerfaces, 192*, Article 111026.

Bureenok, S., Pitiwittayakul, N., Yuangklang, C., Vasupen, K., Saenmahayak, B., Kawamoto, Y., et al. (2019). Evaluation of dried mao pomace (antidesma bunius linn.) and lactic acid bacteria as additives to ensile stylo legume (stylosanthes guianensis ciat184). *JAPS, 29*(3), 783–789.

Cascaes Teles, A. S., Hidalgo Chávez, D. W., dos Santos Gomes, F., Corrêa Cabral, L. M., & Valeriano Tonon, R. (2018). Effect of temperature on the degradation of bioactive compounds of Pinot Noir grape pomace during drying. *Brazilian Journal of Food Technology, 21*(e2017059), 1–8.

Chaaban, H., Ioannou, I., Chebil, L., Slimane, M., Gérardin, C., Paris, C., et al. (2017). Effectt of heat processing on thermal stability and antioxidant activity of six flavonoids. *Journal of Food Processes and Preservation, 41*(5), e13203.

Darici, S., & Şen, S. (2015). Experimental investigation of convective drying kinetics of kiwi under different conditions. *Heat Mass Transfer, 51*(8), 1167–1176.

Demirkol, M., & Tarakci, Z. (2018). Effect of grape (*Vitis labrusca* L.) pomace dried by different methods on physicochemical, microbiological and bioactive properties of yoghurt. *LWT – Food Science and Technology, 97*, 770–777.

Doymaz, I. (2019). Drying of black carrot pomace in an infrared dryer: Kinetics, modelling and energy efficiency. *Sigma Journal of Engineering & Nature Sciences, 37*(1), 71–84.

Endo, H., Higurashi, T., Hosono, K., et al. (2011). Efficacy of *Lactobacillus casei* treatment on small bowel injury in chronic low-dose aspirin users: A pilot randomized controlled study. *Journal of Gastroenterology, 46*(7), 894–905.

Flamini, R., De Rosso, M., & Bavaresco, L. (2015). Study of grape polyphenols by liquid chromatography-high-resolution mass spectrometry (UHPLC/QTOF) and suspect screening analysis. *Journal of Analytical Methods in Chemistry, 350259*.

Guaita, M., Panero, L., Motta, S., Mangione, B., & Bosso, A. (2021). Effects of high-temperature drying on the polyphenolic composition of skins and seeds from red grape pomace. *LWT-Food Science and Technology, 145*, Article 111323.

Janiszewska-Turak, E., Kołakowska, W., Pobiega, K., & Gramza-Michałowska, A. (2021). Influence of drying type of selected fermented vegetables pomace on the natural colorants and concentration of lactic acid bacteria. *Applied Sciences, 11*(17), 7864.

Kammerer, D., Claus, A., Carle, R., & Schieber, A. (2004). Polyphenol screening of pomace from red and white grape varieties (Vitis vinifera L.) by HPLC-DAD-MS/MS. *Journal of Agricultural and Food Chemistry, 52*(14), 4360–4367.

Kara, C., & Doymaz, I. (2015). Thin layer drying kinetics of by-products from pomegranate juice processing. *Journal Food Processes and Preservation, 39*(5), 480–487.

Kayran, S., & Doymaz, Ā. (2019). Infrared drying of apricot pomace. *Latin American Applied Research, 49*(4), 213–218.

Kumar, N., Sarkar, B. C., & Sharma, H. K. (2012). Mathematical modelling of thin layer hot air drying of carrot pomace. *Journal of Food Science and Technology, 49*, 33–41.

Lemus-Mondaca, R., Zura-Bravo, L., Ah-Hen, K., & Di Scala, K. (2021). Effect of drying methods on drying kinetics, energy features, thermophysical and microstructural properties of Stevia rebaudiana leaves. *Journal of the Science of Food and Agriculture, 101*(15), 6484–6495.

Li, W., Wang, M., Xiao, X., Zhang, B., & Yang, X. (2015). Effects of air-impingement jet drying on drying kinetics, nutrient retention and rehydration characteristics of onion (Allium cepa) slices. *International Journal of Food Engineering, 11*(3), 435–446.

Malpeli, A., Gonzalez, S., Vicentin, D., et al. (2012). Randomised, double-blind and placebo-controlled study of the effect of a synbiotic dairy product on orocecal transit time in healthy adult women. *Nutricion Hospitalaria, 27*(4), 1314–1319.

Maskan, M. (2001). Kinetics of colour change of kiwifruits during hot air and microwave drying. *Journal of Food Engineering, 48*, 169–175.

Monteiro, G. C., Minatel, I. O., Pimentel, J. A., Gomez-Gomez, H. A., Correa de Camargo, J. P., Diamante, M. S., et al. (2021). Bioactive compounds and antioxidant capacity of grape pomace flours. *LWT – Food Science and Technology, 135*, Article 110053.

Muhlack, R. A., Potumarthi, R., & Jeffery, D. W. (2018). Sustainable wineries through waste valorisation: A review of grape marc utilisation for value-added products. *Waste Management, 72*, 99–118.

Mujumdar, A. S. (2006). Handbook of industrial drying. In A. S. Mujumdar (Ed.), *Handbook of Industrial Drying*. CRC Press.

Nakov, G., Brandolini, A., Hidalgo, A., Ivanova, N., Stamatovska, V., & Domiv, I. (2020). Effect of grape pomace powder addition on chemical, nutritional and technological properties of cakes. *LWT – Food Science and Technology, 134*, Article 109950.

Ping, E. Y. S., Uthairatanakij, A., Laohakunjit, N., Jitareerat, P., Vongsawasdi, P., & Aiamla-or, S. (2019). Effects of drying temperature and time on color, bioactive compounds, and antioxidant activity in 'Hua Ruea' chili fruit (*Capsicum annuum*). *FABJ, 7*, 1–15.

Ribeiro, C., Freixo, R., Silva, J., Gibbs, P., Morais, A., & Teixeira, P. (2014). Dried Fruit Matrices Incorporated with a Probiotic Strain of Lactobacillus plantarum. *International Journal of Food Studies, 3*(1). Article 1.

Ross, K. A., DeLury, N., Fukumoto, L., & Diarra, M. S. (2020). Dried berry pomace as a source of high value-added bioproduct: Drying kinetics and bioactive quality indices. *International Journal of Food Properties, 23*(1), 2123–2143.

Ross, P. D., & Subramanian, S. (1981). Thermodynamics of protein association reactions: Forces contributing to stability. *Biochemistry, 20*, 3096–3102.

Scartoni, D., Desideri, I., Giacomelli, I., et al. (2015). Nutritional supplement based on zinc, prebiotics, probiotics, and vitamins to prevent radiation-related gastrointestinal disorders. *Anticancer Research, 35*(10), 5687–5692.

Somjai, C., Siriwoharn, T., Kulprachakarn, K., Chaipoot, S., Phongphisutthinant, R., Chaiyana, W., et al. (2022). Effect of drying process and long-term storage on characterization of Longan pulps and their biological aspects: Antioxidant and cholinesterase inhibition activities. *LWT – Food Science and Technology, 154*, Article 112692.

Sui, Y., Yang, J., Ye, Q., Li, H., & Wang, H. (2014). Infrared, convective, and sequential infrared and convective drying of wine grape pomace. *Drying Technology, 32*(6), 686–694.

Taşeri, L., Aktaş, M., Şevik, S., Gülcü, M., Seçkin, G. U., & Aktekeli, B. (2018). Determination of drying kinetics and quality parameters of grape pomace dried with a heat pump dryer. *Food Chemistry, 260*, 152–159.

Teplova, V. V., Isakova, E. P., Klein, O. I., Dergachova, D. I., Gessler, N. N., & Deryabina, Y. I. (2018). Natural polyphenols: Biological activity, pharmacological potential, means of metabolic engineering (review). *Applied Biochemistry and Microbiology, 54*, 221–237.

Vishwanathan, K. H., Giwari, G. K., & Hebbar, H. U. (2013). Infrared assisted dry-blanching and hybrid drying of carrot. *Food Bioproducts Processing, 91*(2), 89–94.

Vivian, J. T., & Callis, P. R. (2001). Mechanisms of Tryptophan Fluorescence Shifts in Proteins. *Biophysical Journal, 80*, 2093–2109.

Zhang, H., Bhunia, K., Kuang, P., Tang, J., Rasco, B., Mattinson, D. S., et al. (2016). Effects of oxygen and water vapor transmission rates of polymeric pouches on oxidative changes of microwave-sterilized mashed potato. *Food Bioprocess Technology, 9*(2), 341–351.

Zhou, L., Xiong, Z., Liu, W., & Zou, L. (2017). Different inhibition mechanisms of gentisic acid and cyaniding-3-O-glucoside on polyphenoloxidase. *Food Chemistry, 234*, 445–454.

Zogzas, N. P., Maroulis, Z. B., & Marinos-Kouris, D. (1996). Moisture diffusivity data compilation in foodstuffs. *Drying Technology, 14*(10), 2225–2253.